

On the design, construction, and testing of a fully-submerged canard hydrofoil system for a low-speed solar boat

AUTHORS

Neola Putnam

119 Glenwood Hwy, Glenwood, WA, 98619
509.364.3333 • ngp32@cornell.edu

Gregory Dickert

108 Turnbull Rd., Cedarville, OH, 45314
443.841.5893 • gp dickert@gmail.com

Caleb Wagner

689 Smith Ave. Apt. 1, Xenia, OH, 45385
717.360.7228 • cwagner@cedarville.edu

Submitted to The International Hydrofoil Society June 2014

*Elmer W. Engstrom Department of Engineering and Computer Science
Cedarville University, Cedarville, OH, 45314*

ABSTRACT

A competition team project to design and build a fully-submerged canard hydrofoil system for a 6 m (18 ft) solar boat was completed to improve craft performance by reducing overall drag. The project focused on three main areas: developing approaches to hydrofoil design using Computational Fluid Dynamics (CFD), improving the manufacture of hydrofoils using infused molding, and achieving foil articulation and flight control with a surface follower mechanism. The CFD work focused on single-phase 2D and 3D analysis of Eppler 420 and Eppler 396 hydrofoil models at low to intermediate Reynolds number using ANSYS Fluent 14.0's inviscid, laminar, and Spalart-Allmaras turbulent models. The half-span of a single hydrofoil was modeled using symmetry to investigate tip vortices and winglet performance. The hydrofoil manufacturing focused on developing a reliable method of manufacturing carbon fiber foils using a vacuum infusion closed-mold process. Medium-Density Fiberboard (MDF) was used for the mold material, and two types of products were tested for mold coating: polyurethane and gelcoat. The foils were composed of aluminum and foam core inserts wrapped in carbon fiber. A lightweight and adjustable mechanical feedback control system actively articulated the front hydrofoils' angle-of-attack and consequently, set boat flying height and maintained craft stability for sustained and self-leveling flight. Independent variable height follower arms attached to water-following skis controlled the angle-of-attack of the front foils. A four-bar linkage system was synthesized to articulate the foil precisely through the full range of motion, from take-off to flying angle-of-attack. Key results of this project were the advancement of the team's CFD hydrofoil modeling practices, the establishment of a reliable carbon fiber foil manufacturing process that yielded foils with excellent surface finish, and a sophisticated foil articulation mechanism. The fully-submerged hydrofoil system as designed and built for the solar boat succeeded as a proof-of-concept design by achieving flight.

TABLE OF CONTENTS

1 – INTRODUCTION	5
2 – METHODOLOGY	7
2.1 <i>Hydrofoil Design and Analysis</i>	7
2.2 <i>Hydrofoil Manufacturing</i>	7
2.3 <i>Articulation and Mounting of Hydrofoils</i>	8
3 – ANALYSIS AND DISCUSSION	8
3.1 <i>Hydrofoil Design and Analysis</i>	8
3.2 <i>Hydrofoil Manufacturing</i>	10
3.3 <i>Articulation and Mounting of Hydrofoils</i>	11
4 – RESULTS	13
4.1 <i>Hydrofoil Design and Analysis</i>	13
4.2 <i>Hydrofoil Manufacturing</i>	16
4.3 <i>Articulation and Mounting of Hydrofoils</i>	17
4.4 <i>Full Hydrofoil System Results</i>	18
5 – CONCLUSIONS AND RECOMMENDATIONS	18
5.1 <i>Conclusions</i>	18
5.2 <i>Recommendations</i>	19
ACKNOWLEDGEMENT	19
REFERENCES	19

LIST OF FIGURES

Figure 1:	Surface piercing and fully submerged foil configurations	5
Figure 2:	Wing Distribution Types	6
Figure 3:	Cross-sectional view of hydrofoil components	7
Figure 4:	Annotated right side of articulation and mounting system assembly	8
Figure 5:	Foil Connection Bracket	8
Figure 6:	C-grid mesh of Clark-Y airfoil	10
Figure 7:	Front and rear foils as used in the final design	10
Figure 8:	2D winglet meshes	10
Figure 9:	Mesh of 3D wing with 3D winglet	10
Figure 10:	Diagram of vacuum infused closed mold process	11
Figure 11:	Hydrofoil Manufacturing Schedule	11
Figure 12:	Design tree used to categorize designs to vary the hydrofoil's AOA	12
Figure 13:	Foil Connection Block oriented on its side	12
Figure 14:	Front foil strut	12
Figure 15:	Foil connection and Link 3 assembly	12
Figure 16:	Ski and turnbuckle assembly	12
Figure 17:	Mounting block assembly	12
Figure 18:	Chart depicting profile selection	13
Figure 19:	Laminar model of Clark-Y airfoil	13
Figure 20:	Lift coefficient for Eppler 387 experimental and CFD results	14
Figure 21:	Drag coefficient for Eppler 387 experimental and CFD results	14
Figure 22:	Lift coefficient for Eppler 420 (front foil) CFD results	14
Figure 23:	Drag coefficient for Eppler 420 (front foil) CFD results	14
Figure 24:	Lift coefficient for Eppler 396 (rear foil) CFD results	14
Figure 25:	Drag coefficient for Eppler 396 (rear foil) CFD results	14
Figure 26:	Half-wing planforms used in the single 3D foil taper and aspect ratio study	15
Figure 27:	Percentage amount the coefficient of lift and drag change when comparing a 2D "infinite wing" to a finite 3D wing for different wing taper and aspect ratio wings	15
Figure 28:	Percent difference in C_L and C_D for 3D wing with and without winglets	15
Figure 29:	Wingtip vortices streamlines from a 3D wing with a square winglet	16
Figure 30:	Three-point bend test set-up	16
Figure 31:	Hydrofoil's three-point bend test results as completed on the Instron machine	16
Figure 32:	Aluminum hydrofoil core with threaded rod	16
Figure 33:	Mold with cutouts made to fit the aluminum core with threaded rod	17
Figure 34:	Layup process with carbon fiber	17
Figure 35:	Front foil with foil connection bracket and strut	17
Figure 36:	Full front hydrofoil and articulation mechanism assembly	18
Figure 37:	Hydrofoil boat in take-off and flight	18

1 – INTRODUCTION

The 2012-2013 Cedarville University Solar Boat Team competed in the annual Solar Splash World Championship held in Cedar Falls, IA in June 2013. Two faculty advisors (one mechanical and one electrical) supervised the project. The team was composed primarily of senior mechanical engineers who chose Solar Boat for their senior capstone project. For the competition, each team designs and builds a human-skippered, battery and solar powered boat for on-the-water events that test their boat's maneuverability, speed, and endurance. During the high-speed Sprint event, Cedarville's boat is powered by a 36 V battery system capable of providing 31.8 kW (42.6 hp). The Endurance event is powered by a solar array allowed to produce up to 480 W (0.65 hp) under a one-sun condition, in addition to a 24 V battery system of 432 W (0.59 hp). In consideration of the limited allowable power, the individual boat systems of a successful design: solar array, peak power tracker, controls, motor, gearbox, propeller, and hull must meet efficiencies specified by an overall power budget, shown in Table 1, without sacrificing craft performance.

Table 1. Power Budget for Solar Splash Endurance Event (Numbers in far-right-hand column refer to power output for that component and input specifications for the next downstream component.)

System Component	Voltage (V)	Current (A)	Component Power Gain (W)	Output Power (W)		
Solar Array	48.0	7.00	336	336		
Peak Power Tracker (MPPT)	23.4	13.64	-16.8	319		
Batteries	23.4	18.00	421	421		
Controls	23.4	31.6	-37.0	703		
	Torque		Angular Velocity		Component Power Gain (W)	Power (W)
Motor	N*m	lbs*ft	rad/s	rpm	-91.4	612
	1.95	1.44	314.2	3000		
Gear Box	Torque		Angular Velocity		Component Power Gain (W)	Power (W)
Gear Ratio=	N*m	lbs*ft	rad/s	rpm	-30.6	581
	5	9.25	6.82	62.8		
	Thrust		Velocity		Component Power Gain (W)	Power (W)
	N	lb	km/hr	mph	-81.4	500
Prop Hull	131.6	29.6	13.68	8.50		
					-500	0.00
Efficiencies	MPPT	Controls	Motor	Gear Box	Prop	
	95.0%	95.0%	87.0%	95.0%	86.0%	

Per Solar Splash competition rules [1], returning teams are allowed to use work completed by their team in

previous years. Usually, the Cedarville team focuses on a few key goals each year, building on previous work. The main goal of the 2013 team was to develop a working hydrofoil system by incorporating Computational Fluid Dynamics (CFD) and aerodynamic theory as design tools, manufacturing the hydrofoils via an infusion mold process, and developing a low weight, streamlined articulation mechanism. The system was designed for the Endurance Event; teams could apply the same principles to design hydrofoils for other events and competitions. Based on the weight of the craft and skipper, as well as the power budget (Table 1), the following design specifications were derived for the 6 m (18 ft) boat:

- The Endurance Event configuration hydrofoils must be able to lift the boat and driver, 2890 N (650 lb), such that the hull is completely out of the water at a speed of 13.7 km/hr (8.5 mph), while incurring a drag less than or equal to 132 N (29.6 lb).
- To meet overall weight goals, the combined weight of the front and back hydrofoils is not to exceed 111 N (25 lb).
- The variable lift system must maintain lift for the entire duration of the race and the combined weight of the entire articulation and mounting system should not exceed 90 N (20 lb).

At flying speed, a boat with hydrofoils can be more efficient than a conventional boat because if the foils lift the boat out of the water, they can reduce the drag force. In general, the forces acting on the hydrofoil (far from any free surface boundaries) can be expressed using the same fluid dynamic theories applicable to airplane wings. The main difference between airplane and hydrofoil theory is the presence of a free-surface interface above a hydrofoil. O'Neill [2] has provided a succinct overview of hydrofoil boat design, including topics on foil design, stability, and lift control. Vellinga [3] has outlined a foil design process based on aerodynamic theory.

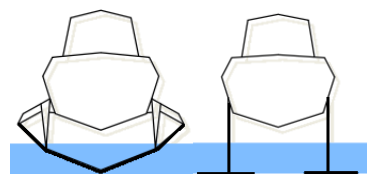


Figure 1. Surface piercing and fully submerged foil configurations (Wikipedia)

Two factors contribute significantly to foil design: foil configuration and weight distribution. Hydrofoils are classified as surface piercing or submerged, as shown in Figure 1. Surface piercing hydrofoils generally are simpler to design and implement because they self-stabilize and control lift by varying the submerged area but are less efficient because the lift force acts at an

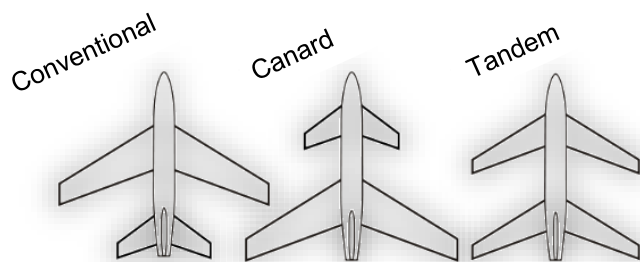


Figure 2. Wing Distribution Types (*Wikipedia*)

angle offset from vertical. Submerged foils are efficient but not self-stabilizing. Weight distribution depends on the relative size of the forward and aft foils. In a conventional configuration, the front foils support 65% or more of the boat and driver's weight, the rear foils support the majority of the weight in a canard configuration, and the tandem configuration is one where the weight is distributed evenly between the foils. These distributions are shown in Figure 2. As investigated by Latorre and Singkorn [4], other aspects of hydrofoil design, including foil size and angle, also affect hydrofoil behavior.

CFD is dedicated to the study of fluids in motion, whose physical characteristics can be described using the governing continuity and Navier-Stokes differential equations. Hepperle [5] developed an online applet JavaFoil, which uses the panel method (a subset of potential flow theory) coupled with boundary layer analysis, to calculate the flow field and friction drag, respectively, on a 2D airfoil as defined by a series of points. Many other numerical methods exist to obtain solutions to predict flow behavior around hydrofoils. Roohi, Zahiri, and Passandideh-Fard [6] simulated cavitation around a 2D foils using the Volume of Fluid (VOF) method and Large-Eddy-Simulation (LES) turbulence model. The commercial CFD code ANSYS Fluent 14.0 [7] solves the non-linear mass and momentum conservation equations using either a pressure-based solver that relies on a projection method or a density-based solver that couples the mass and momentum equations and solves using an implicit or explicit linearization. As a design tool, CFD is desirable because it potentially can predict performance before the design is even manufactured and implemented.

Previous Cedarville teams have used a variety of methods to manufacture hydrofoils. In 2006, the first foils were constructed with a wood core and layered with fiberglass for strength [8]. The cores were modeled in SolidWorks and machined on the CNC. Although the method showed some promise, the results were less than satisfactory: the wooden cores resulted in an inaccurate foil profile that took too long to hand-finish. The second method, used in 2007, employed foam cores with a fiberglass overlay. This boat suffered from "tail squat"

behavior due to backwash from the front surface piercing hydrofoil [9]. An aluminum hydrofoil was incorporated with a displacement hull and used in 2011 [10]. The hope was to provide some lift to reduce hull drag, but the difference was negligible, if not counter-productive. The 2012 team constructed the foil with a CNC machined aluminum core and a carbon fiber exterior [11]. Using a CNC machined, closed mold of the hydrofoil shape, the aluminum core and carbon fiber material were vacuum infused with resin. However, the 2012 team was unable to perfect the manufacturing process. Their foils exhibited numerous surface voids where the resin had not entirely filled the mold. The team filled and sanded the voids by hand, but this was a tedious process and the structural integrity of the foil was still questionable where those voids were present. The main concern regarding hydrofoil manufacturing is how one builds a structurally sound and dimensionally accurate foil that can be manufactured reliably within a few days.

Articulating and mounting the hydrofoils is as important as hydrofoil design. According to Vellinga [3], without some means of varying lift, hydrofoils are dynamically unstable. They cannot fly at a constant height above the water's surface, but rather, cycle through a positive feedback loop. When lift increases from an increase in speed, the bow gains height and increases the angle-of-attack (AOA), which further increases lift. Eventually, the front foil either stalls or egresses out of the water. When this occurs, lift decreases until the boat returns to the state where the motor can supply adequate power to increase the speed enough to restart the cycle.

Stability and appropriate flying height can be achieved through several different methods. The use of a variable lift front foil is the most common method of controlling stability and flying height for smaller crafts. There are many ways to vary the lift of the front foils. A few of these methods include employing spoilers, changing the wetted area of the foil (e.g., surface piercing foils), varying the AOA, or changing the flap angle of the foil. The AOA can be controlled automatically or by human input, much like piloting an airplane. At the 2012 DONG Solar Energy Challenge in the Netherlands, some teams incorporated a ski-like height sensor on submerged front hydrofoils, which skimmed on the water's surface. The mechanism varied the AOA so that AOA was greatest when water's surface was at the boat hull (prior to takeoff) and then decreased until equilibrium was achieved (lift equals weight). Finally, some workers, such as the team from TU Delft at the DONG Challenge have devised programmable systems that measure the instantaneous boat height and vary the hydrofoil AOA accordingly with an electric motor.

The strategy and results for designing and incorporating hydrofoils on the Cedarville Solar Splash boat in Endurance configuration is discussed in this paper. Section 2 presents the method of approach for the three areas of focus: hydrofoil design and analysis, hydrofoil manufacturing, and hydrofoil mounting and articulation. A brief description of some of that CFD analysis, discussion of manufacturing techniques, and synthesis and analysis of the articulation mechanism is presented in Section 3. The key findings and successes of the results and testing are included in Section 4. Finally, in Section 5, hydrofoil feasibility for this particular application and recommendations for future workers are discussed.

2 – METHODOLOGY

2.1 Hydrofoil Design and Analysis

The purpose of modeling hydrofoils using CFD was to predict how parameters such as foil profile, span, aspect ratio, and taper affected performance and tip vortex energy losses. The commercial meshing program, ICEM, and modeling program, ANSYS Fluent 14.0, were selected as analysis tools. Early on, JavaFoil [5] was used to obtain an estimate of foil sizing such that work could begin on developing the infusion molding process.

In the initial design, JavaFoil was used to determine lift and drag coefficients for a given foil profile. Given Equation (1), the entire lift force of a foil can be calculated. The expression for drag force is similar to that for lift: the lift coefficient merely is changed to a drag coefficient.

$$L = \frac{1}{2} \rho u^2 A C_L \quad (1)$$

where ρ is the fluid density, u is hydrofoil velocity, A is planform area (area projected onto the chord plane), and C_L or C_D are lift or drag coefficient, respectively. The power budget in Table 1 shows that the boat speed, based on available battery and solar power, is relatively limited. Since lift is proportional to the square of velocity, at lower speeds, the planform area and lift coefficient must be relatively large to ensure enough

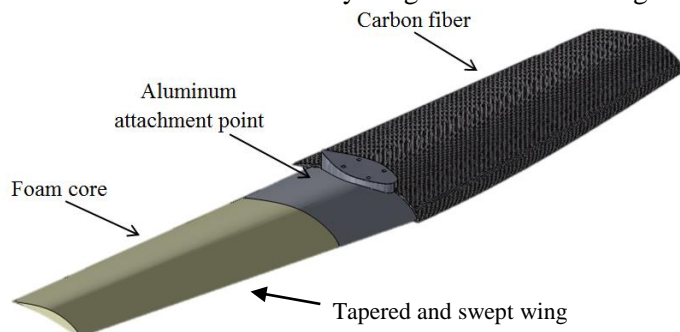


Figure 3. Cross-sectional view of hydrofoil components.

force is generated to lift the hull out of the water. JavaFoil was used to determine foil profiles that have a high lift coefficient as well as relatively high lift to drag ratio, as these indicate that the profile displays good lifting characteristics without incurring drag in excess of the available thrust.

With an approximate design in place, effort was directed toward meshing and running models in Fluent. The first CFD models consisted of 2D foil profiles in single phase fluid flow: the profiles being the Clark-Y, Eppler 387, and the two profiles selected in the earlier analysis. The Clark-Y results were compared to pressure coefficient curves from a Cedarville undergraduate junior-level wind tunnel lab experiment and the Eppler 387 lift and drag coefficients were compared to those found by McGhee, Millard, and Walker [12].

To improve the analysis, studies were conducted using a 3D foil model. A 2D hydrofoil represents a 3D wing of infinite span, but this representation cannot capture the effects of wingtip vortices, which are known to decrease foil lift and increase drag. A parametric study of foil taper and aspect ratio was conducted to determine how geometry affects performance by reducing vortices.

Once these vortices were observed in the CFD model, winglets were added to investigate the potential for improving lift and decreasing induced drag. First, 2D planar winglets of different sizes were modeled to determine an effective winglet shape. Finally, a 3D winglet was meshed in ICEM.

2.2 Hydrofoil Manufacturing

As discussed in the background section of this paper, Cedarville Solar Splash boat teams have attempted several methods of hydrofoil manufacturing: wood core with fiberglass coating, foam core with fiberglass coating, aluminum, and aluminum core with carbon fiber outer layers. The carbon fiber option was considered the most viable because this material is lightweight and has excellent tensile strength. To manufacture the foils, a vacuum-infused closed mold process was selected because it has the capability to produce identical parts multiple times.

As in 2011-2012, an aluminum core insert was CNC machined to act as the attachment point for the extruded aluminum airfoil-shaped struts used to attach the hydrofoils to the boat. Additionally, CNC machined foam cores were included on either side of the aluminum insert to fill out the hydrofoils without adding excessive weight. The cut-away of a typical hydrofoil is given in Figure 3.

Several hydrofoil iterations were completed in the process of perfecting the manufacturing process. First,

two different mold coatings, polyurethane and gelcoat, were used to determine which yielded a better foil surface finish. Secondly, a trial hydrofoil was subjected to a three-point bend test to determine if the selected number of carbon fiber layers was sufficient to withstand the bending stress the foil would experience during flight. Thirdly, as the hydrofoils were resized using better design techniques, larger molds and foils required more rigorous molding techniques.

2.3 Articulation and Mounting of Hydrofoils

In the past, the Cedarville solar boat team has only employed surface piercing hydrofoils to vary lift and adjust the height of the foils. In 2013, the team desired an efficient means of varying lift of a fully submerged system via a mechanism on the front foils. The method of varying the front hydrofoils' AOA using a surface following ski was selected based on the success other hydrofoilers have attained on boats similar in size to Cedarville's.

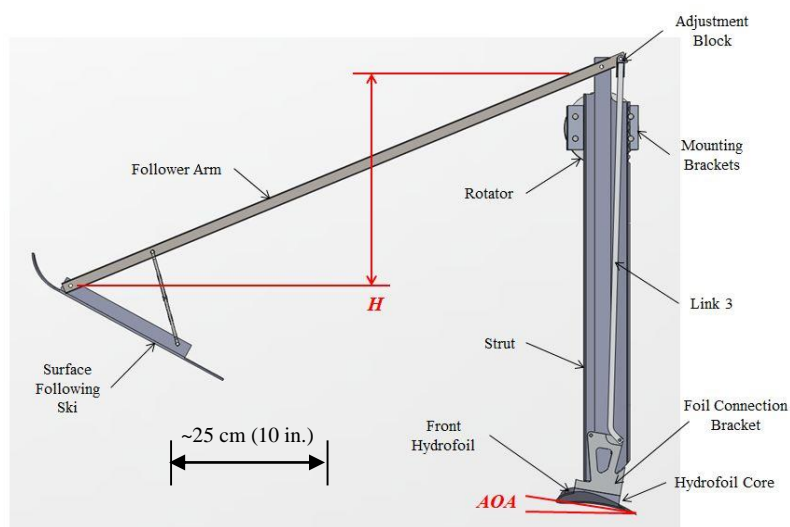


Figure 4. Annotated section view of right side of articulation and mounting system assembly.

Several design configurations could be used to vary the AOA using a surface follower. Using a design tree method to compare and contrast various options, a design was selected whereby a four bar linkage pivots the front foil midway on the strut (Figure 12). The linkage was synthesized using kinematic methods given boundary conditions of AOA at takeoff and cruise, as well as the distance from the top of the hull to the water and the submerged distance of the foil at cruise. A force analysis was also conducted to determine the forces applied on the pins and the planning force the water exerts on the ski. These would be used to constrain motion of the mechanism by appropriately sizing the ski and determine the required diameter of the pins. The detailed design of the mechanism assembly is shown in Figure 4.

With that analysis complete, the individual components were designed based on the following overarching principles, in no particular order. First, a light, but precise design was desired since “slop” in the system could cause undesirable, rapid changes in AOA. Second, for ease of fine-tuning the mechanism's settings, adjustability in a few components was important. Third, to reduce drag, the flow around the submerged components should be relatively undisturbed. Fourth, the components were designed for ease of disassembly to stow the system in the hull during Sprint events. Finally, the components were designed for manufacturing simplicity.

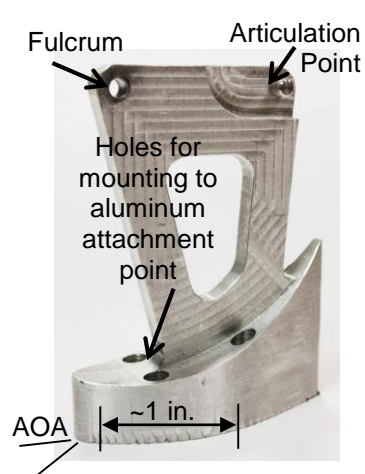


Figure 5. Foil Connection Bracket

Using these principles, the components were created and assembled in the CAD tool, SolidWorks. This phase was useful especially for designing the front foil connection bracket shown in Figure 5: the fulcrum of the entire articulation and mounting system.

The rear foil connection was simpler to design because it does not articulate. In place of the connection bracket, an adapter piece was created to mount to the aluminum core. It was design specifically with simplicity and a lower weight in mind.

The front and rear foil struts were mounted to the hull using the same type of mounting blocks. These mounting blocks were designed for two purposes: rigidly attaching the hydrofoils to the hull and transferring the lift forces to the hull. They transferred the load from the foils through the strut by clamping the strut within the blocks. A positive stop was included in the strut to keep it from slipping out.

3 – ANALYSIS AND DISCUSSION

3.1 Hydrofoil Design and Analysis

The pressure and velocity fields surrounding a body (e.g., a hydrofoil) in a flow field allow one to predict behaviors like lift and drag. In the case where an analytical solution is complicated or even impossible to obtain, the Finite Volume Method (FVM) is used. The physical problem of interest includes a domain of fluid with known material properties flowing around a hydrofoil subject to certain boundary conditions. CFD

analysis is an approximate one: assumptions are made to transform the physical problem into a mathematical model for which a solution can be obtained.

Given a physical domain or control volume, the VOF method divides it into small control volume cells, whose common points are called nodes. At each of the cell centers, the velocity and pressure field are calculated using a mathematical algorithm. This is a numerical solution, and as such, error is produced. Methods of reducing error might include creating a finer mesh or using smaller time steps in an unsteady analysis.

The two equations fundamental for fluid analysis are the mass and momentum conservation equations. The general form of the mass conservation equation in indicial notation is given by (2) and is applicable to compressible and incompressible flows.

$$\frac{\partial \rho}{\partial t} + \frac{\partial \rho u_j}{\partial x_j} = S \quad (2)$$

The first term represents the unsteady rate of change of mass within a control volume. This is important in transient simulations. The second term represents the convection of mass across cell faces, and u_j is the velocity of the flow field. The source term S is applicable in case of multiphase flow, where the dispersed second phase adds mass to the continuous carrier phase. In all simulations conducted for this project, the source term was zero. The general form of the momentum conservation equation in a non-accelerating reference frame is given by (3) in indicial notation.

$$\frac{\partial \rho u_i}{\partial t} + \frac{\partial \rho u_i u_j}{\partial x_j} = -p \delta_{ii} + \frac{\partial \tau_{ij}}{\partial x_j} + \rho g_i + F_i \quad (3)$$

where p is the fluid pressure, δ_{ii} is the unit tensor, τ_{ij} is the stress tensor given by (4), ρg_i is the gravitational body force, and F_i represents external body forces.

$$\tau_{ij} = \mu \left[\left(\frac{\partial u_i}{\partial x_j} + \frac{\partial u_j}{\partial x_i} \right) - \frac{2}{3} \frac{\partial u_i}{\partial x_i} \delta_{ij} \right] \quad (4)$$

where μ is the molecular viscosity and δ_{ij} is the Kronecker delta. The momentum equation describes how the unsteady effects of momentum (first term on LHS) combine with the convection of momentum (second term on LHS) to balance the pressure gradient, divergence of shearing stress, and gravitational and body forces.

Within the Fluent program, there are several flow models for the various fluid flow regimes. The important number that characterizes the flow around a hydrofoil is

the Reynolds number: the non-dimensional ratio of inertial to viscous forces. It is given in Equation (5):

$$Re = \frac{\rho u C}{\mu} \quad (5)$$

where C is the characteristic length of the object of interest (i.e., the chord length). For the simulations completed, the hydrofoil was approximated as a flat plate to estimate the Reynolds number at which flow transitioned from laminar to turbulent: $Re = 5 \times 10^5$. Laminar flow, $Re < 5 \times 10^5$, is characterized by the fluid flowing in streamlined layers with little to no disruption between these smooth layers: viscous forces are more dominant than inertial forces. In the case of a higher velocity or longer chord length (assuming the fluid properties remain the same), the Reynolds number is increased. If the flow surpasses the transition point, random turbulent eddies tend to appear in the flow, disrupting the wake region behind the foil. Another model of interest is the inviscid model. This model assumes that viscous forces can be neglected; physically, this corresponds to very high Reynolds number flows. It can be useful as a flow initialization model (later switching to a more complex turbulent model) or as an estimate for flow behavior. Based on the Reynolds number, one should select the flow model appropriately.

The inviscid model calculates the flow field using potential flow theory (which was developed based on the assumption that the flow field is inviscid). The laminar flow model approximates the solution to be inviscid in the general flow field, and at the boundary layer along the hydrofoil, uses laminar boundary layer theory to approximate the viscous effects. The Fluent program supports several turbulent models; the one of interest for this project was the Spalart-Allmaras (SA) model.

According to the ANSYS Fluent Theory Guide [13], the SA model works well for simulations where the flow boundary layers have an adverse pressure gradient, and that it was developed for aerospace applications with wall-boundary flows. At the shoulder, or high point of the foil's camber, an adverse pressure gradient commences. The SA model solves only one modeled transport equation: the kinematic eddy (turbulent) viscosity. As such, results could be obtained relatively quickly and were representative of the flow within the desired accuracy.

The following is a discussion of how these principles were applied to the hydrofoil analysis conducted by the team. As discussed in the methodology section, JavaFoil was used to conduct a preliminary study quickly to determine a design that could be used to manufacture the first foil. The hydrofoil system was specified to be a canard with split front foils. Additionally, fully

submerged foils were selected because this style is more efficient and has a better chance of achieving flight. In regards to the overall goals specified by the power budget, this simplified design was predicted to provide a lift of 294 kg (650 lb) and incur a drag of 15 kg (33 lb).

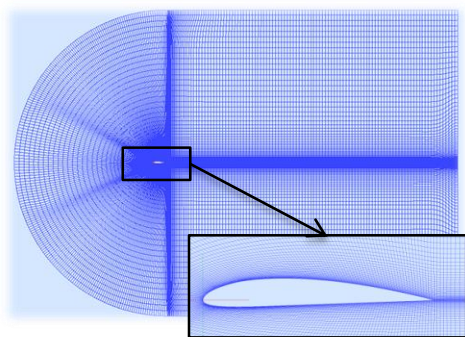


Figure 6. C-grid mesh of Clark-Y airfoil

From the JavaFoil analysis, two airfoil profiles were selected: the Eppler 420 profile for the front foils and the Eppler 396 for the rear foil. The coordinates used to

represent these two foils, as well as the two foils who were used as a data validation set (the Clark-Y foil for the laminar model and the Eppler 387 for the turbulent models) were obtained from the University of Illinois airfoil database [14]. Figure 6 provides a snapshot of the C-grid mapped mesh used for these airfoils.

With the single 2D foil Fluent models validated, the analysis was extended into 3D hydrofoils. Four combinations were compared, using tapers of 0.7 and 0.9 and aspect ratios, or ratio of hydrofoil span to chord length, of 10 and 14. A hydrofoil design less favorable to tip vortices would allow for smaller winglets. However, boat specifications limited the span of the front foils: consequently, they still had a low aspect ratio. The final design selection is provided in Figure 7. Unfortunately, experimental (or theoretical) data sets were unavailable with which to compare to the 3D results. Therefore, the best available strategy was to match the simulation

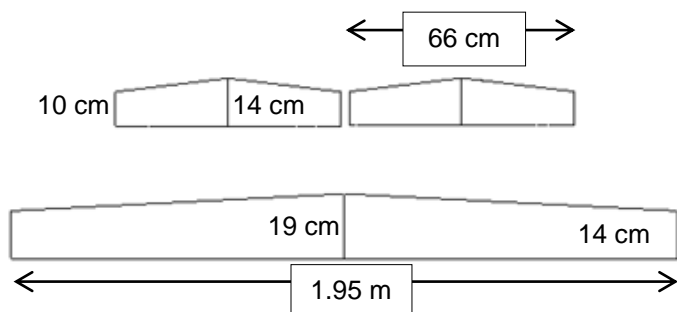


Figure 7. Front and rear foils as used in the final design.
Front Foils (Eppler 420): 5.50 AR and 0.71 taper
Rear Foil (Eppler 396): 11.9 AR and 0.74 taper

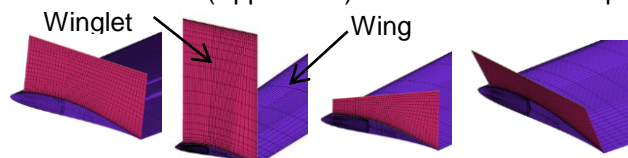


Figure 8. 2D winglet meshes (from L to R): square winglet, tall square winglet, triangle winglet, and square winglet at a 60° cant angle.

models and methods as closely as possible to the 2D models completed earlier.

To offset trailing vortices, winglets can be installed to provide inward side forces that block the outward fluid motion along the top of the hydrofoil. A study modeling 2D winglets on a 3D hydrofoil half-span was completed for four different representative winglet shapes. The winglets shown in Figure 8 were added to the rear Eppler 396 profile foil, and the hydrofoil was modeled using the inviscid solver. Note that the Reynolds number of 5×10^5 to 7×10^5 normally would have been represented by a turbulent model; however, the purpose of this model was to obtain a qualitative understanding (not quantitative) of how well different winglet shapes could offset vortices. Thus, the inviscid model was used to reduce computational time. The front foils were not modeled with vortices because they are very close to each other at the inside tips. Winglets would likely increase interference drag such that the improvement of reduced induced drag were offset by the increased interference drag. This winglet study was meant to show qualitatively that winglets improve performance.

As a further investigation of winglet performance, a 3D winglet was added to the CAD model and the meshing strategy shown in Figure 9 was developed. The winglet profile used by Richard T. Whitcomb in his 1976 winglet study [15] was selected arbitrarily for this meshing scheme. The goal of such a study was to investigate how much a 3D winglet modeled with one of Fluent's turbulence models would have a higher friction drag due to the viscous forces now being included. However, the study has not yet been completed.

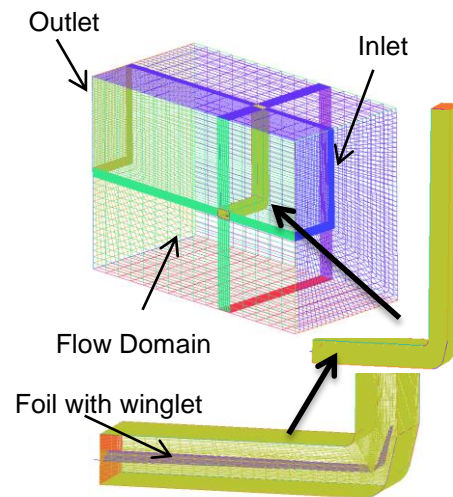


Figure 9. Mesh of 3D wing with 3D winglet. Fluid flows in the inlet, past the wing, and exits via the outlet.

3.2 Hydrofoil Manufacturing

The key hydrofoil manufacturing goals were to develop a reliable manufacturing process and then manufacture and test the hydrofoils. The vacuum infused closed mold process selected for the project was a type of Resin Transfer Molding: a diagram of the mold and foil is shown in Figure 10. The hydrofoil (carbon fiber laid up

on a solid core) is placed into a closed mold, and a vacuum draws resin in to the mold until the resin infuses the entire part. The part conforms to the mold shape.

Medium-Density Fiberboard (MDF) was selected as the mold material because it is inexpensive and can easily and relatively quickly be machined into the desired shape. Professional closed molds typically are made with fiberglass. These molds are stronger and more durable; however, they take longer to make and require more costly materials. MDF is a quite soft material, but a hydrofoil mold must have a hard surface for mold strength and accurate surface finish. Therefore, two mold coatings were tested on different molds: polyurethane and gelcoat. Polyurethane is less expensive and is easy to apply. However, hydrofoils do not de-mold well from molds coated with polyurethane, and often the mold is destroyed during de-molding. The molds lined with gelcoat had a thicker and tougher coating: one that held together better when de-molding the hydrofoils.

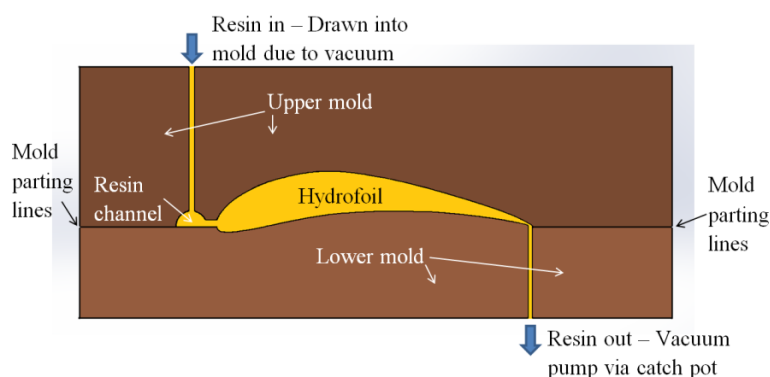


Figure 10. Diagram of vacuum infused closed mold process.

The hydrofoil was made from carbon fiber wrapped around a core of foam and aluminum pieces. Figure 3 in Section 2.2 shows the foam core, aluminum attachment piece, and the carbon fiber in cutaway. The strategy of including core sections was used because a solid carbon fiber hydrofoil requires much more fiber for the same part—this is unnecessary, expensive, and adds weight. Also, it would be difficult to lay up a solid carbon fiber hydrofoil and ensure an accurate hydrofoil profile. When using a closed mold, the carbon surrounding the core must completely fill the mold to avoid the presence of voids. However, overfilling or under-filling must be avoided, as these will lead to flaws in the foil as well. Aluminum was selected as the center attachment material to provide, as a solid connection, additional strength. The medium density foam core was selected primarily to save weight and fiber material while serving as a form upon which to lay up carbon. The foam did not add strength to the part except possibly to prevent buckling of the upper skin in compression. Both the aluminum and foam cores were machined using a CNC. The use of core material ensures the desired profile

shape and simplifies the lay-up of carbon fiber while still providing sufficient strength.

Once the core material was prepared, the carbon fiber was laid up on the core. Primarily, unidirectional carbon fiber was used because the maximum stress occurs along the hydrofoil's longitudinal direction. In flight, the hydrofoil's bottom surface experiences tension and the top compression. To exploit carbon fiber's superior tensile strength, during lay-up it was ensured that the fibers on the bottom were aligned longitudinally. The longitudinal alignment of carbon fiber on top was not as critical because the resin—not the carbon fiber—takes most of the compressive stresses. One layer of “45° - 45°” carbon fiber was included to help counter any torsional stresses the hydrofoil would experience in operation.

With the carbon fiber lay-up complete, the hydrofoils were infused. Mold release agents were applied to the molds to improve the de-molding quality. After the hydrofoil was infused and removed from the mold, some finishing work was required. Typically, the hydrofoils had excess resin around the edges that required sanding down. The foils were coated with a varnish and polished to a smooth finish in preparation for testing and use. The timetable for manufacturing a hydrofoil is summarized in Figure 11.



Figure 11. Hydrofoil Manufacturing Schedule

3.3 Articulation and Mounting of Hydrofoils

Though not used by previous Cedarville solar boat teams, the 2013 team desired to develop a fully submerged configuration with a mechanical control system to vary lift. The design tree mentioned in Section 2.3 used to categorize different possibilities of pivoting the front foils is provided in Figure 12. The selected path is highlighted by bold orange arrows. The option where the foil pivots about an imaginary point, as shown in Figure 12(A), requires greater forces from the ski and a more complicated attachment scheme. Placing the pivot on the foil, as shown in Figure 12(B), caused the entire lift load to be transferred through a pin inside the foil. There likely would not be enough room for a pin strong enough to fit within the foil. On the other hand, pivoting the entire strut, as in Figure 12(D), would cause the lift force's location to vary. Therefore, a four bar linkage to

pivot the front foil midway on the strut, as illustrated in Figure 12(C), was selected as a compromise of designs B and D. This design also allowed us to locate the linkage within the strut, keeping the flow as undisturbed as possible.

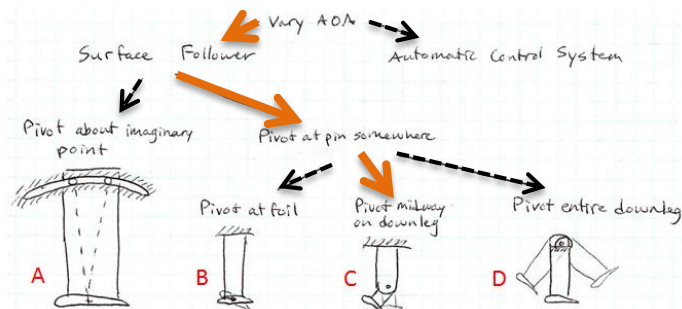


Figure 12. Hand sketch of design tree from the designer's log book, used to categorize similar designs that could be used to vary the hydrofoil's AOA.

Next, the four bar linkage was synthesized using kinematic theory. The boundary condition at takeoff was a height from top of the hull to the water of 26.5 cm (10.4 in) and foil AOA of 14° . At cruise, the height was designed to be 58 cm (22.8 in) for adequate hull clearance above the water and an AOA of 1° for optimal lift/drag characteristics. A TK Solver code was written to synthesize a linkage that would follow the desired range of motion. A force analysis was conducted to determine the forces in the pins, the force necessary to constrain motion of the hydrofoil, the minimum moment inertia required of Link 3, and the minimum diameter of the pins. It was determined that only about 44.5 N (10 lb) of force is necessary to keep the ski on the water's surface. Such a force does not require a large ski when the boat is traveling at 14 km/hr (8.5 mph). The force analysis also specified the required diameter of the pins. Finally, a buckling analysis of Link 3 (see Figure 4) was completed to determine that the minimum allowable diameter for the link is 9.5 mm (0.37 in).

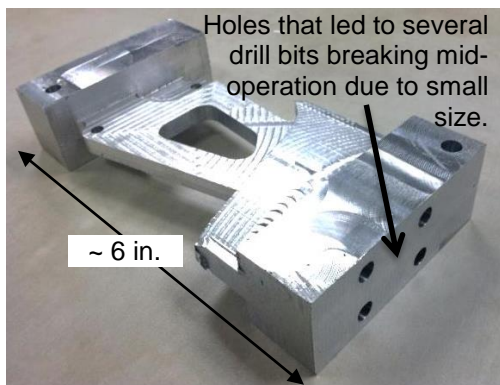


Figure 13. Foil Connection Block oriented on its side.

With the necessary analysis complete, and with the design principles outlined in Section 2.3, the individual components were designed.

The Link 3 with adjustment block assembly, shown in Figure 4, was designed to be one of the components that

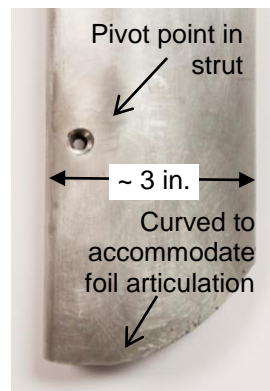


Figure 14. Front foil strut

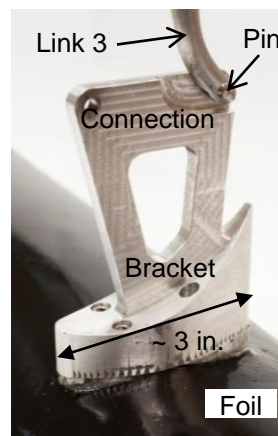


Figure 15. Foil connection and Link 3 assembly

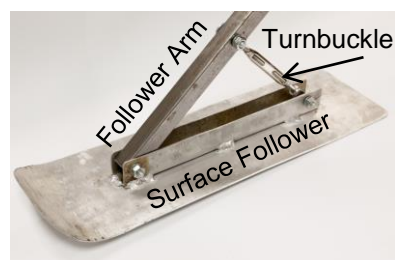


Figure 16. Ski and turnbuckle assembly



Figure 17. Mounting block assembly

would allow adjustability in the system. The foil connection bracket is shown in Figures 5 and 13: it proved to be the most challenging component to design and manufacture. The distance from the holes in the bottom of the clamping blocks to the top of the strut cross-section was quite long and resulted in several drill bits breaking mid-operation. The issue was resolved by drilling through the clamping block portion with a much larger drill bit, increasing spindle speed, and using cutting oil. The front foil strut, which housed the articulation mechanism and attached the foil to the boat, is shown in Figure 14. The strut end radius and the pin hole were cut using the CNC milling machine for precision. Two portions of aluminum round stock were welded in the pin holes. After drilling, tapping, and counterboring the hole, the extra material was removed. The two stock pieces function as positioning blocks for the foil connection, add bearing area and space to countersink the head of the pin within the strut, and constrain the foil connection laterally.

Once the components were manufactured, the foil connection was mounted on the hydrofoil. In Figure 15, the foil, connection bracket, and Link 3 are shown in their assembly. A pin connecting the foil

connection and Link 3 is held in place by an interference fit. After Link 3 is slipped on the pin and the foil connection is inserted in the strut, there is no space for Link 3 to slip off the pin because the walls of the strut are close. The ski and follower arm, pictured in Figure 16,

were designed with a turnbuckle connecting them to allow a wide range of adjustment of the ski's AOA. Thus, the ski's water surface finding characteristics can be optimized.

The mounting blocks attaching the front and rear foil struts were similar to the one shown in Figure 17. The mounting blocks also allow some height adjustability as the positive stop pin on the blocks is inserted in notches in the strut. The notches allow strut height adjustability and transfer the lift force to the hull.

4 – RESULTS

4.1 Hydrofoil Design and Analysis

The JavaFoil results for lift to drag ratio of several representation foils is given in Figure 18. The Eppler 396 was chosen for the rear foil because it displayed the best lift to drag ratio of the foils that were investigated, and the Eppler 420 for the front foils because even though it did not display as high a lift to drag ratio as the Eppler 396, it maintained a good ratio throughout the full range of AOA, from 1° to 14° , whereas the Eppler 396 foil's dropped significantly part-way through that range.

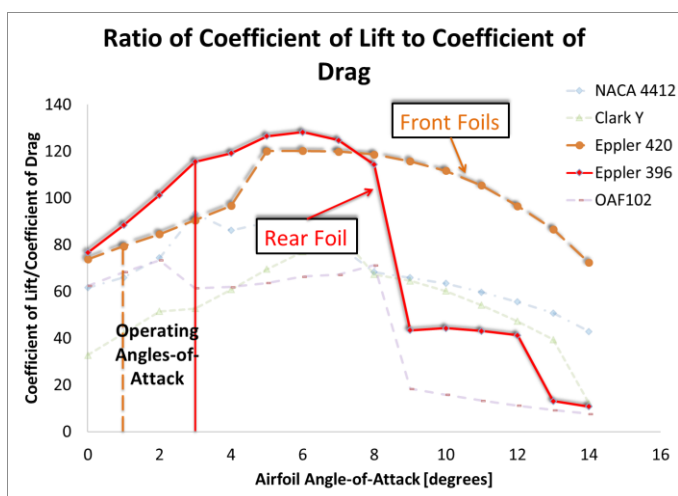


Figure 18. Chart depicting profile selection

Fluent was used to solve the 2D single phase model for the Clark-Y, Eppler 387, 396, and 420 for varying angles-of-attack and obtain the following solutions. The experimental data available for the Clark-Y airfoil was the pressure distribution given by the square symbols in Figure 19. The plot shows the value of pressure coefficient around the airfoil. One can see the experimental results correlating well with the laminar Fluent model: the results given for a Reynolds number of approximately 1.24×10^5 . The spike in data at the upper trailing edge is a result of flow separation and was expected for an airfoil set at an angle-of-attack. It also can be observed that the mesh, when refined from 35,500 nodes to 120K (as completed for the 2° AOA in Figure 19), does not lead to a significant change in the

model's results. Therefore, it was concluded that the mesh was sufficiently fine for the results to be considered mesh independent, and that the laminar model would be an appropriate model for low Reynolds number flows.

The slightly higher Reynolds number rear foil was predicted to operate near the point at which flow transitions from laminar to turbulent. Therefore, experimental wind tunnel data [13] of coefficient-of-lift and coefficient-of-drag were obtained for AOA from 0° to 7° at $Re = 4.6 \times 10^5$. This data is plotted in Figures 20 and 21 along with the results from Fluent's inviscid and SA models.

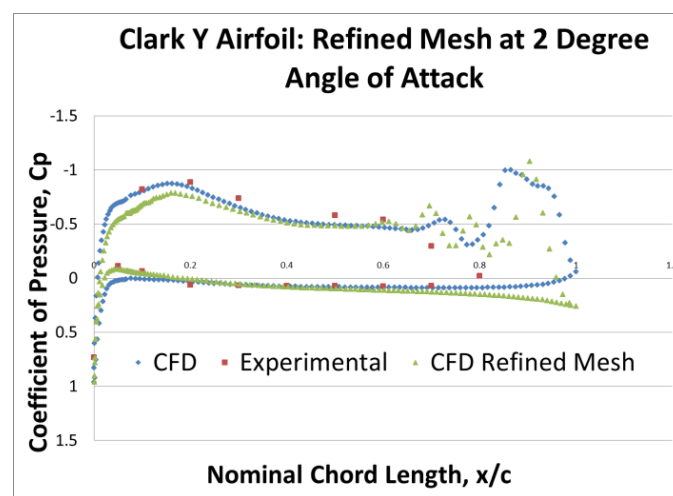


Figure 19. Laminar model of Clark-Y airfoil. Coarse and refined meshes match experiment fairly well.

Note that neither model reports values in agreement with the coefficient-of-drag experimental results; however, they follow the same slight upward trend. By taking the average of the inviscid and SA models, CFD predictions close to the experimental values were obtained. This strategy is not usually the norm, but it was decided that because the foil was predicted to be in the transition range, no model would be able to capture the turbulent effects completely, and that taking the average would be a legitimate assumption for Reynolds number around this value.

Next, using the modeling strategies developed with the Clark-Y and Eppler 387, the Eppler 420 front foil ($Re = 2.27 \times 10^5$) and the Eppler 396 rear foil ($Re = 5.3 \times 10^5$) were simulated as well. Results for the coefficients of lift and drag are given in Figures 22 - 25. It was observed that the JavaFoil applet overpredicts coefficient of lift and significantly underpredicts coefficient of drag, compared to Fluent's laminar model. This is because boundary layer theory (which JavaFoil uses to estimate drag coefficients) assumes an operating regime of relatively high Reynolds number.

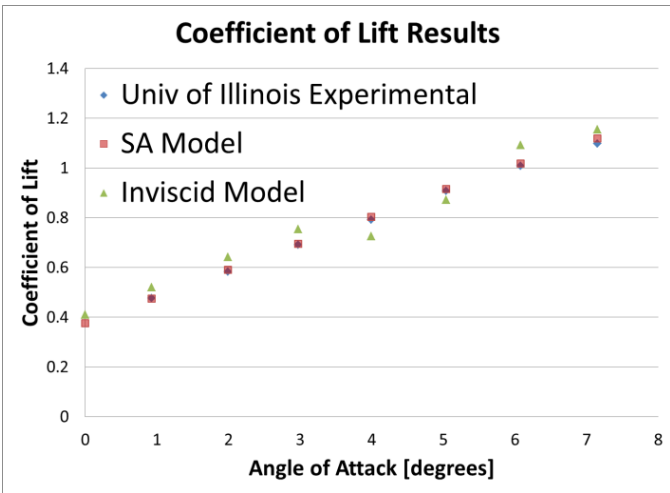


Figure 20. Lift coefficient for Eppler 387 experimental and CFD results. $Re = 4.6 \times 10^5$

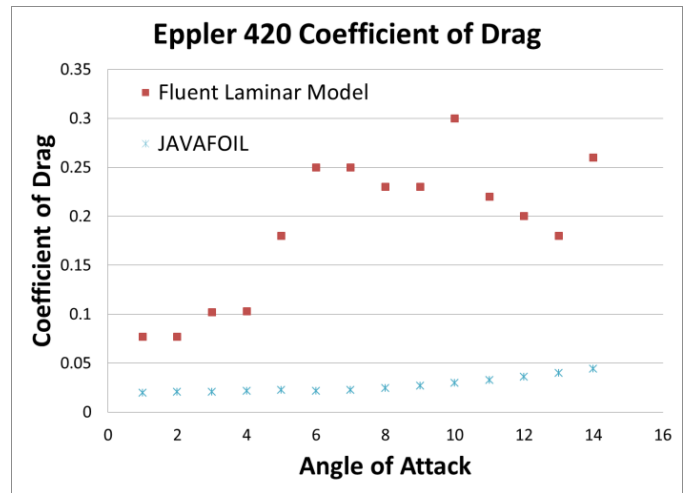


Figure 23. Drag coefficient for Eppler 420 (front foil) CFD results. Note how JavaFoil cannot accurately predict drag coefficient for laminar flow.

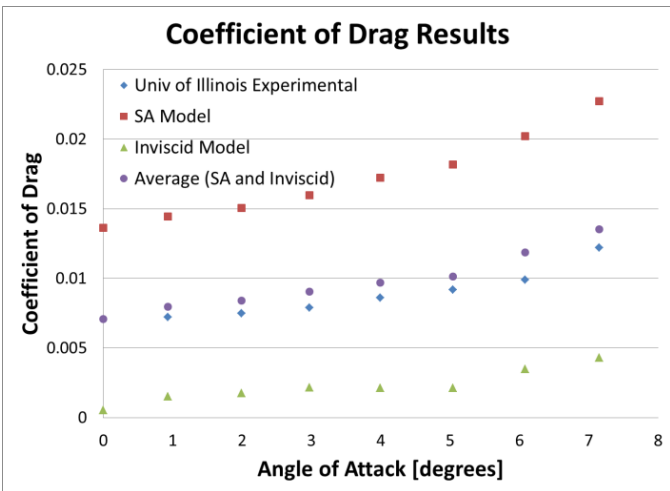


Figure 21. Drag coefficient for Eppler 387 experimental and CFD results.

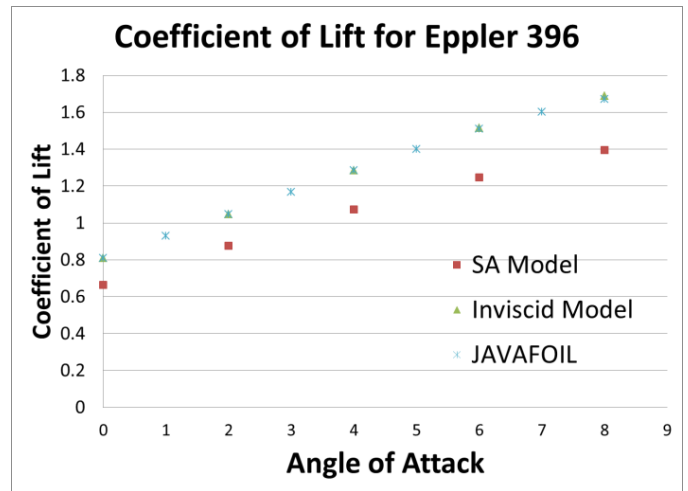


Figure 24. Lift coefficient for Eppler 396 (rear foil) CFD results. $Re = 5.3 \times 10^5$

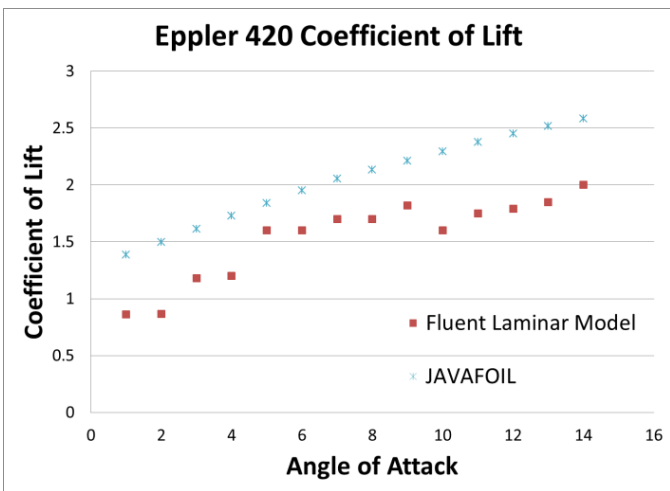


Figure 22. Lift coefficient for Eppler 420 (front foil) CFD results. $Re = 2.27 \times 10^5$

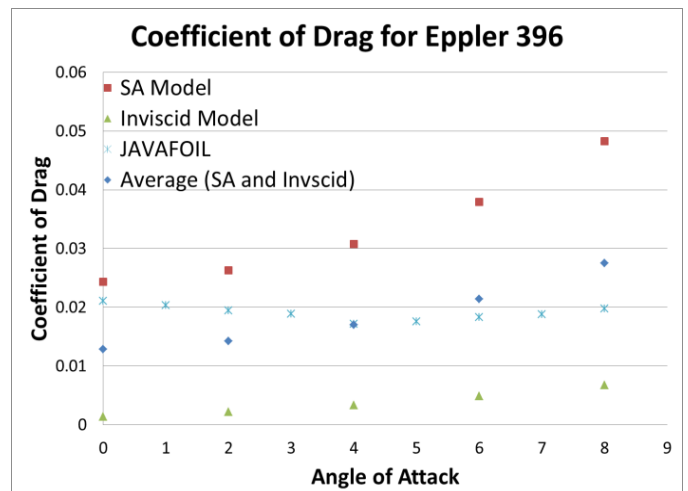


Figure 25. Drag coefficient for Eppler 396 (rear foil) CFD results. The drag coefficient used was the average of the inviscid and SA models.

For the study in which wing taper and aspect ratio were varied for a 3D hydrofoil, the combinations shown in Figure 26 were applied to the Eppler 396 profile. As shown in Figure 27, the



Figure 26. Representative sketches of half-wing planforms used for the single 3D foil taper and aspect ratio study.

induced drag from the tip vortices drastically reduces wing performance compared to the 2D model. As expected, high aspect ratio hydrofoils have the best performance: drag and lift are affected the least when compared to a 2D airfoil model. However, increase in aspect ratio is limited by the structural integrity of the foil; as the foil span increases and chord length remains constant, bending stress will increase. Additionally, the front foils were designed with their inside tips so close to each other that their spans could not be further increased. However, it was desired to maintain separate front foils because the foil articulation system has better roll stability with split front foils.

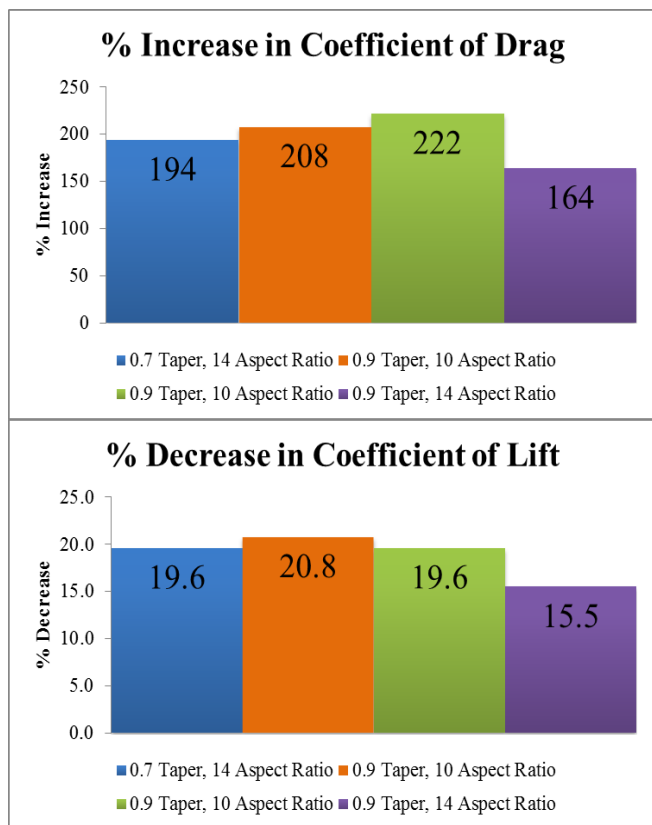


Figure 27. Percentage amount the coefficient of lift and drag change when comparing a 2D "infinite wing" to a finite 3D wing for different wing taper and aspect ratio wings.

The 3D hydrofoil with 2D winglet study showed that differences in winglet size and shape have an effect on how well the winglet reduces wingtip vortices. A qualitative analysis was completed by modeling the flow around the rear Eppler 396 foil using only the inviscid solver (neglects viscous effects). The four winglet designs were compared with the inviscid Fluent results of the 3D wing without a winglet to determine which winglet provides the greatest improvement in lift and drag coefficients conditions at the desired operating AOA (3°) and Reynolds number (6×10^5). The results are summarized in Figures 28 and 29. The winglet set at a 60° cant angle (winglet is tipped outward 60°) and a medium-sized rectangular winglet reduce drag the most of these four designs and provide a reasonable amount of lift improvement.

The final hydrofoil design as manufactured used the coefficients of lift and drag obtained from the 3D single phase single foil simulations. The early foil profile choices of the Eppler 420 for the front and Eppler 396 for the rear were maintained. The total predicted lift at 13.7 km/hr (8.5 mph) for this design was 1961 N (440.8 lb) and the total predicted drag (including the attachment struts to the foils) was 246 N (55.3 lb). Throughout the year, the size of the hydrofoils was modified several times as the CFD modeling increased in complexity.

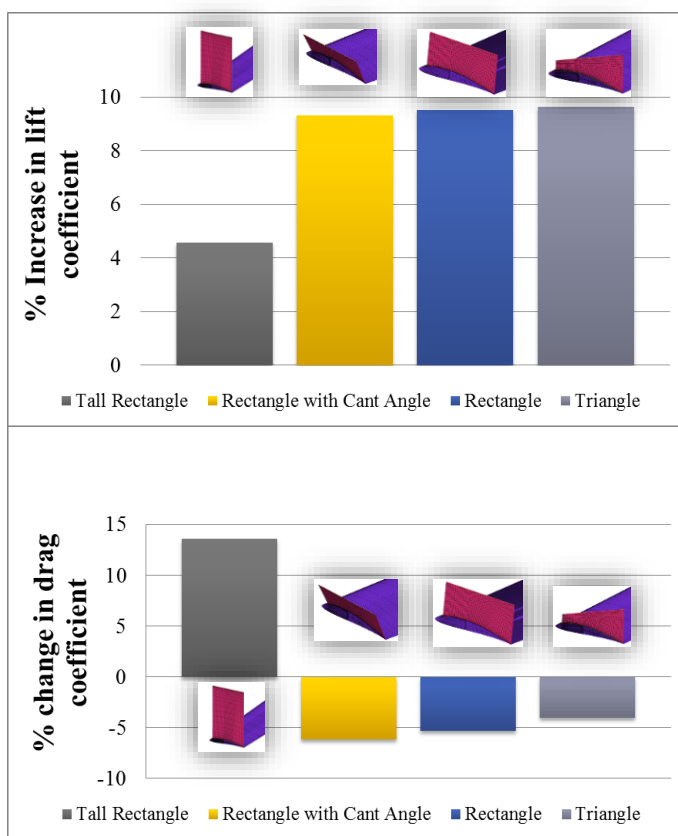


Figure 28. Percent change in C_L and C_D for 3D wing with 11.8 AR and 0.74 taper ($Re = 6 \times 10^5$) with attached 2D winglets compared to wing without.

This modeling allowed the changes to be made without full-scale testing at all iterations because it provided an indicator of how the foils should perform.

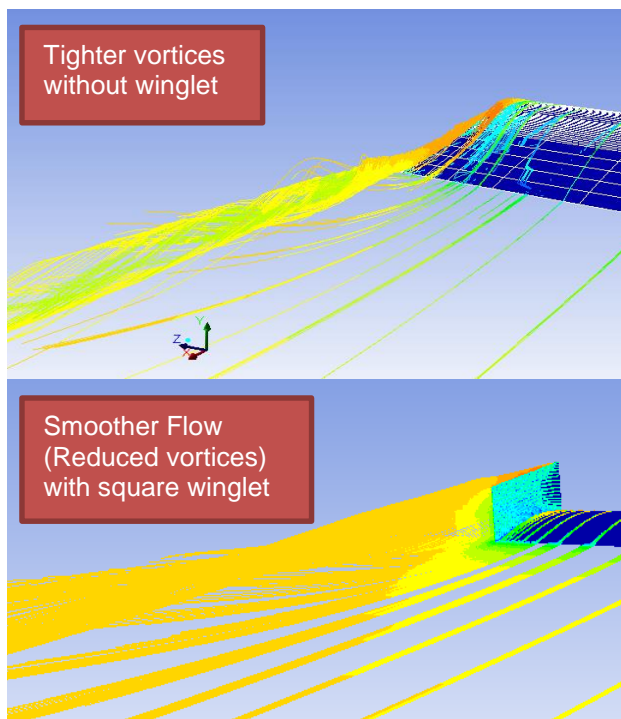


Figure 29. Wingtip vortices streamlines from a 3D wing with a square winglet at simulated velocity of 8.5 mph (11.8 aspect ratio and 0.74 taper wing). The colors correspond to different velocity magnitudes.

4.2 Hydrofoil Manufacturing

The foil produced in first foil manufacturing iteration displayed some imperfections, but the overall quality of the foil was much improved compared to the 2011-2012 teams' efforts. The objective of this iteration was to practice the carbon fiber lay-up and infusion process, so the aluminum attachment core was not included. The major flaw of this iteration was that the trailing edge of the foil was rough. This was a result of not clamping the two mold pieces together as tightly as necessary. Another problem encountered was that during demolding, the bottom half of the mold was destroyed and could not be reused. The polyurethane mold sealant was not strong enough to protect the weak MDF board material—the mold pulled apart from itself with minimal applied force and stuck to the hydrofoil.

A three-point bend test was performed on the first hydrofoil to determine if the number of carbon fiber layers was adequate and if the hydrofoil could withstand the 334 N (75 lb) lift force corresponding to the design prediction for that iteration. The test set-up is shown in Figure 30 and the results in Figure 31. It was determined that the hydrofoil supported approximately 578 N (150 lb). This test could be considered conservative based on the fact that the supports were located at the ends of the hydrofoil, out past the location of the hydrofoil's center-

of-pressure, the resultant force location of the lifting pressure force. As a result, the bending stress was larger than it would be in operation. Though the foil exceeded the required loading, it was decided to use more carbon layers on future iterations to further improve the foils' safety factor.

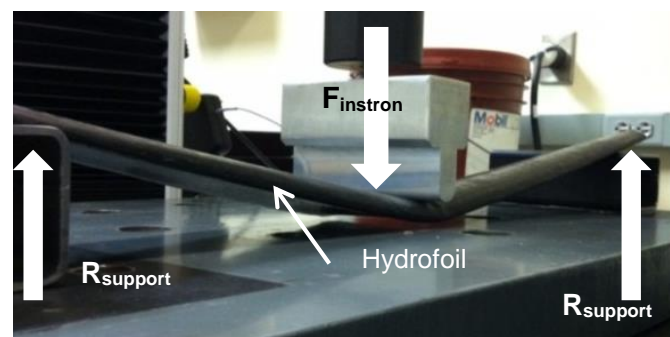


Figure 30. Three-point bend test set-up

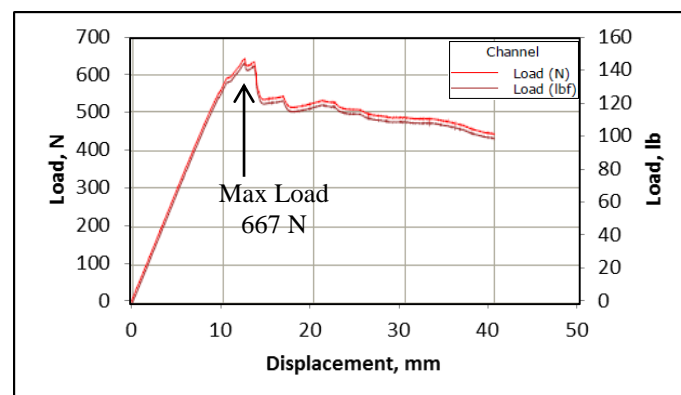


Figure 31. Plot of the hydrofoil's three-point bend test results as completed on the Instron machine

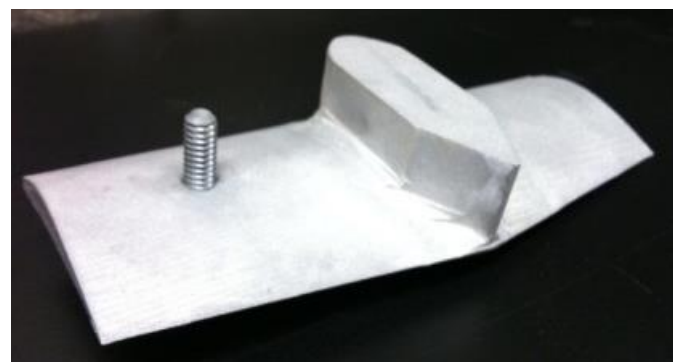


Figure 32. Aluminum hydrofoil core with threaded rod

The second hydrofoil manufacturing iteration used the same foil design as the first hydrofoil. The difference was that the aluminum attachment was included to make this a more realistic version. A threaded rod was included that protruded out of the aluminum attachment through the top of the foil to provide an AOA reference position. The aluminum core is shown in Figure 32. The

mold constructed to accommodate the threaded rod and strut profile is shown in Figure 33.

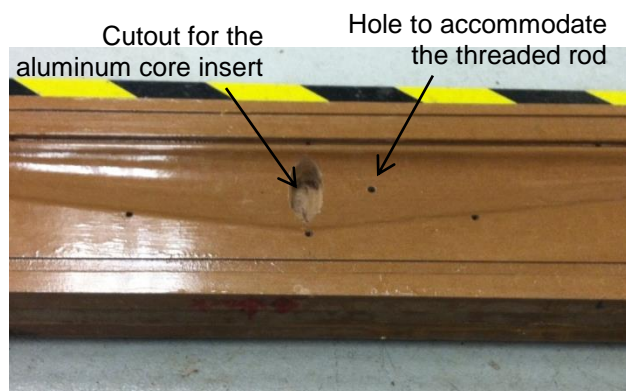


Figure 33. Mold with cutouts made to fit the aluminum core with threaded rod

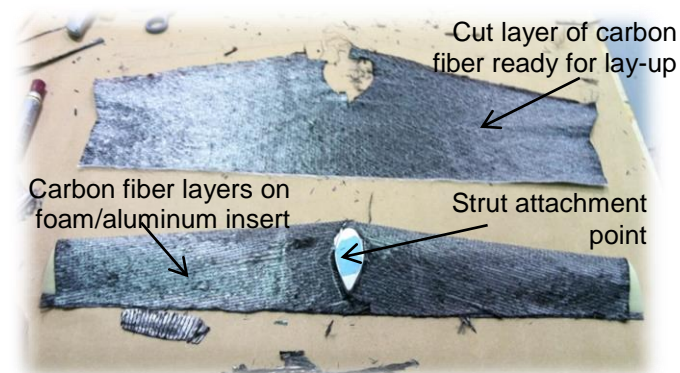


Figure 34. Layup process with carbon fiber

With the mold and aluminum insert completed, the second hydrofoil was laid up with carbon fiber, in a manner similar to that shown in Figure 34, and the part was infused. A minimum of 4 and up to 7 layers of carbon fiber was used. Unfortunately, the second hydrofoil was even more difficult to de-mold than the first, and once again, the mold was destroyed in the de-molding process. The aluminum strut profile and threaded rod, which protruded into the mold, provided the mold with more surface area with which to hold the hydrofoil. Additionally, there were too many layers of carbon fiber wrapped around the core, overfilling the mold. The two halves of the mold separated slightly and provided a gap that filled with resin during infusion. This resin held the mold together. One difference between the two manufacturing iterations was that the bottom half of the mold was coated gelcoat. The bottom mold held together better during de-molding than the mold sealed with polyurethane.

The third iteration molds and foils were much larger in span, chord length, and thickness than the previous two iterations. At the time of manufacturing, gelcoat was unavailable; polyurethane was used again as the mold coating in combination with a wax layer. Between the

second and third iteration, the use of a threaded rod was discontinued because the top surface of the aluminum core insert is parallel to the hydrofoil's zero AOA and can be used as the reference plane instead. The height of the aluminum core that protruded out of the carbon fiber was decreased to provide less surface area for the mold to cling to. However, significant issues were still experienced when de-molding the foil: most likely as a result of polyurethane being used for the mold coating.

On the fourth foil manufacturing iteration, the molds were completed for both the front and rear foils—these were the largest foils made thus far. The molds were completely coated with gelcoat for this iteration: a significant improvement was observed in de-molding. Not only did the foils come out easily, but they also exhibited excellent surface finish. The final surface finishing steps were completed, and the hydrofoils were ready for testing.

4.3 Articulation and Mounting of Hydrofoils

The front foil with mounting mechanism and strut attached is shown in Figure 35, and Figure 36 displays the full articulation system assembly for one of the front hydrofoils with the foil attached. The task requirements specified that the total weight of the articulation and mounting system be less than 89 N (20 lb). A single front assembly weighed 27.6 N (6.2 lb); thus, the total weight of the front system was 55.2 N (12.4 lb). Since the rear foils contain fewer parts (e.g., follower arm, ski, link 3, etc.), this assembly weighs less, meeting the weight requirement. The final design is streamlined and moves smoothly through the range of motion. The linkage was tested to confirm that it achieves the desired AOA at a given surface follower height. Finally, it was confirmed that the system could be adjusted via the intended components: length of Link 3, ski angle (via the turnbuckle), and the submerged depth of the foils. With the articulation system complete, it was used to mount the hydrofoils to the boat.

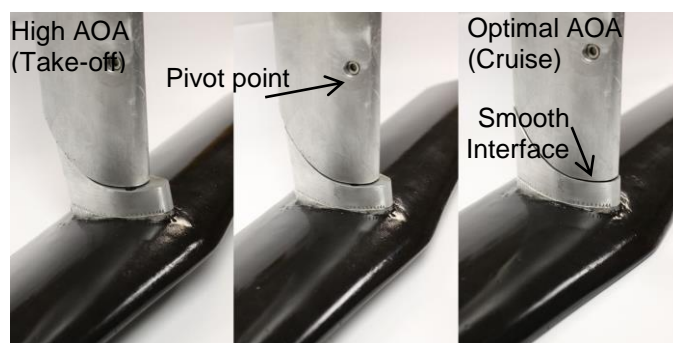


Figure 35. Front foil with foil connection bracket and strut. The images show a progression of decreasing AOA's from the takeoff to cruise. The design of this connection was chosen because it reduces flow disturbance around the connection.

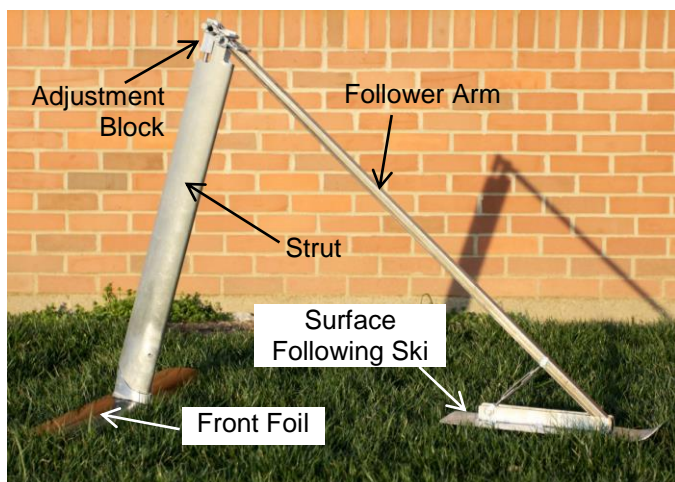


Figure 36. Full front hydrofoil and articulation mechanism assembly.

4.4 Full Hydrofoil System Results

The final design prediction of lift the foils could attain at 8.5 mph was 1961 N (440.8 lb) with a total predicted drag of 246 N (55.3 lb). However, in the Endurance racing configuration, the foils would need to provide a lift of 2880 N (650 lb) without incurring a drag in excess of 132 N (29.6 lb) as determined by the weight of the craft and the power budget. Therefore, it was decided to test the design as a proof-of-concept with as few of the



Figure 37. Hydrofoil boat in take-off and flight.

components in the boat as possible: with the driver, the weight of the boat was approximately 1912 N (430 lb). The work the 2013 team completed was the first use of fully submerged foils, and it was desired to test the viability for this application.

Testing on a lake approximately 200 m long, it was found that the boat could take off on the hydrofoils and maintain flying height much more reliably than past Cedarville teams accomplished using surface-piercing configurations. The boat rose at a fairly level angle and did not experience the “tail squat” problem that the 2007 team experienced in their testing [10]. Figure 37 captures a few still images of take-off and flight from video taken during testing. Unfortunately, the lake used for tested in was not long enough to observe extended sustained flight, nor was it wide enough to turn the boat without “falling” back down onto the hull. However, the team was pleased with the overall results of the proof-of-concept testing.

5 – CONCLUSIONS AND RECOMMENDATIONS

5.1 Conclusions

A competition team project to design and build a working hydrofoil system for a Solar Splash boat Endurance configuration was completed with three main areas of focus: developing approaches to hydrofoil design using CFD, improving the manufacture of hydrofoils using infused molding, and achieving foil articulation and flight control with a surface follower mechanism. Future boat teams may apply the principles and processes developed to other events and other competitions.

The Hydrofoil Design sub-team developed the Cedarville University boat team’s capabilities of using CFD as a design tool via a two-fold method. First, by learning this tool and using it to create designs used by the rest of the team for that year, and secondly, by providing helpful documentation regarding the use of the CFD programs for future Cedarville team analysts to use as a guide. The team focused on simple models such as single phase 2D airfoils and 3D hydrofoils using the most basic flow models (i.e., laminar model, inviscid model, and Spalart-Allmaras turbulence model). The work also included some meshing and modeling of 2D and 3D winglets on a 3D hydrofoil. This work was meant to expand the knowledge of tools available for design and analysis.

The Hydrofoil Manufacturing sub-team focused on perfecting a reliable and relatively rapid method of manufacturing foils. A vacuum infusion closed-mold processes was used to make the foils because such a method has the capability of producing identical parts

multiple times with a good surface finish. Medium-Density Fiberboard (MDF) was used for the mold material, and two types of products were tested as a mold coating: polyurethane and gelcoat. Gelcoat proved to be the superior product. The foils were composed of aluminum and foam core inserts wrapped in a carbon fiber exterior. The manufacturing process as developed, greatly improved upon the one used by the 2012 team.

The Hydrofoil Articulation sub-team concentrated on designing an innovative hydrofoil mounting and articulation system. To achieve sustained and self-leveling flight, a system was designed to actively control the front hydrofoils' angle-of-attack and consequently, the boat flying height, with a mechanical feedback control system. This system consists of independent variable height follower arms attached to water-following skis, which control the angle-of-attack of the front foils. A four-bar linkage system was designed to fit within the foil mounting strut so the mechanism could achieve the desired range of angles without disturbing the fluid flow. The design includes an adjustable rear foil attachment. In the design process, the focus was to create a mechanism that was lightweight and adjustable, allowed precision control, could be disassembled rapidly, and was relatively simple to manufacture.

The 2012-2013 team's main contribution to the Cedarville solar boat legacy was the design and manufacturing processes used to make a working hydrofoil system.

5.2 Recommendations

Future CFD work should focus on understanding and documenting the fluid mechanics behind the computational code and how different settings change the physical boundary and initial conditions of a problem. There is a temptation to run a model and present the results without considering how the code obtained the reported results; however, this limits understanding the accuracy of the results and how they can be applied in design. Additionally, it is important to understand the type of information pertinent to present in a report of CFD results (i.e., domain size, qualitative and quantitative error analysis, critique of the numerical model, etc.). These two areas are key to the reliability of the results and demonstrate that the method is meaningful.

Regarding hydrofoil CFD analysis, one area of importance is that of understanding the free surface effect on a hydrofoil's ability to produce lift. As the foil nears the surface, lift tends to decrease to the point that none is being produced. Additionally, near the surface of the water, wave drag, as created by the hydrofoil deforming the water's surface, decreases the available power for forward travel. Unlike for an aircraft wing,

which experiences only single phase flow, the free surface effect experienced when a hydrofoil travels near the water's surface should be an important concern.

In regards to the hydrofoil manufacturing process, there are two areas of possible improvement. First, the manufacturing process of hydrofoils should be accelerated if possible: reducing the time it takes to go from CAD model to finished product from nearly a week to two or three days. Such an improvement would be valuable when testing several foil design iterations. Secondly, it would be beneficial to develop a method to check how closely the final hydrofoil product matches the desired profile shape. Lifting ability of a hydrofoil is strongly affected by slight modifications in the foil profile. Improvements in the manufacturing process should improve foil quality and product reproducibility.

Finally, the design created for the Endurance configuration in 2012-2013 would be unable to lift the entire required load for the full duration of the Endurance race due to limitations of overall drag and available power. Given the limited amount of power, a combination of weight reduction and hydrofoil design improvement will have to be conducted to allow hydrofoil use to be feasible for the Endurance Event configuration. Though the boat was able to fly in a "proof-of-concept" configuration, it would not be successful in an actual Endurance Event competition.

ACKNOWLEDGEMENT

The authors wish to thank Dr. Tim Dewhurst, Dr. Gerald Brown, Dr. George Qin, and Mr. Wayne Leffingwell for their expertise and invaluable guidance in support of this project. The work was completed as a senior design project at Cedarville University.

REFERENCES

- [1] Solar Splash Rules Committee, "2013 Solar Splash Competition Rules." Accessed May 2013. http://www.solarsplash.com/spl_rule.php
- [2] W. O'Neill "Hydrofoil Ship Design." (Dec 2004).
- [3] R. Vellinga, *Hydrofoils: Design Build, Fly*. Peacock Hill Publishing, (2009).
- [4] R. Latorre, Singkorn Teerasin, Calculation of hydrofoil craft take-off speed including influence of foil size, foil angle and propeller shaft angle, *Ocean Engineering*, Vol. 19, Issue 2, (March 1992) 183-197.
- [5] M. Hepperle, JavaFoil Online Applet. Last accessed 16 Jan 2014. <http://www.mh-aerotoools.de/airfoils/javafoil.htm>
- [6] E. Roohi, A. Zahiri, M. Passandideh-Fard, Numerical simulation of cavitation around a two-dimensional

hydrofoil using VOF method and LES turbulence model, *Applied Mathematical Modelling*, Vol. 37, Issue 9, (May 2013) 6469-6488.

[7] ANSYS Fluent 14.0 program. (Nov 2011)

[8] S. Danielsen, T. Dewhurst, D. Foster, B. Hill, J. Hague, N. Miller, J. Oliver, M. Redfield, R. Woodward, M. Zermiski, S. Ziegenfuss. "2005-2006 Solar Boat Team Final Report" (2006).

[9] J. Reichert, M. Dotson, C. Shanks, J. Boston, M. Hubenthal, J. Winter, J. Conyers, M. Veldt, J. Briggs, S. Smith, T. Dewhurst. "2006-2007 Solar Boat Team Final Report" (2007).

[10] J. Bierer, J. Conway, J. Dewhurst, A. Hensler, A. Koch, D. LaCroix, and T. Smidt. "2010- 2011 Solar Boat Team Final Report" (2011).

[11] A. Koch, E. Lamb, J. Oakes, K. Nicolaisen, S. McLeod, T. Poore, N. Rogers, T. Ronco, W. Sorensen, Z. Ziegler, and B. Yeh. "2011- 2012 Solar Boat Team Final Report" (2012).

[12] R. McGhee, B. Millard, B. Walker, Experimental results for the Eppler 387 airfoil at low Reynolds numbers in the Langley Low-Turbulence Pressure Tunnel [Washington, DC]: National Aeronautics and Space Administration, Scientific and Technical Information Division (1988).

[13] *Theory Guide for ANSYS Fluent 14.0*. ANSYS, Inc. (2011).

[14] UIUC airfoil coordinates database. (Jan 2013). Last accessed 17 Jan 2014. http://aerospace.illinois.edu/m-selig/ads/coord_database.html.

[15] R. Whitcomb, A Design Approach and Selected Wind-Tunnel results at High Subsonic Speeds for Wing-Tip Mounted Winglets, Langley Research Center. (1976): 1-30.

Mechanical Designer for elevators. He plans to pursue a MBA in engineering management in the near future.

Caleb Wagner is currently working as a crew systems engineer for the United States Air Force at Wright-Patterson AFB. Beginning fall 2014, he will be attending Purdue University, pursuing a M.S.M.E. His work on hydrofoil control at Cedarville University inspired him to focus his graduate studies on dynamics, controls, and design.

Neola Putnam recently completed her Master of Engineering degree in Mechanical Engineering at Cornell University. Starting summer 2014, she will be working as a Research and Development Engineer for Proctor and Gamble's FemCare department. She received her bachelor's degree in Mechanical Engineering from Cedarville University.

Gregory Dickert worked as a manufacturing engineer transitioning into the shop operations manager at JMS Composites of Springfield, OH the past year after graduating from Cedarville University with a bachelor's degree in mechanical engineering. He recently accepted a position with Fujitec America Inc. in Mason, OH as a